atmosphere

MDPI

Article

Seasonal Changes of Extremes in Isolated and Mesoscale Precipitation for the Southeastern United States

Thomas Rickenbach

Department of Geography, Planning and Environment, East Carolina University, Greenville, NC 27858, USA; rickenbacht@ecu.edu; Tel.: +1-252-328-1039

Received: 1 July 2018; Accepted: 7 August 2018; Published: 9 August 2018

Abstract: The association between instantaneous extreme precipitation and mesoscale organization over the southeastern United States is not well known. This study addresses whether isolated precipitation features have a distinct distribution and spatial pattern of extreme rain compared to mesoscale precipitation features, and how these distributions and spatial patterns change from spring to summer. Using a four-year surface radar precipitation data set, hourly images of instantaneous extreme rain rates were separated into isolated and mesoscale precipitation features from March through August for the four-year period of 2009–2012. Results show that that compared to isolated convection, mesoscale precipitation organization is more commonly associated with higher extremes in instantaneous rainfall in the southeastern U.S. Extreme rain values tied to mesoscale organization shift eastward and toward the coasts from spring to summer, while extreme rain from isolated convection is mainly a summer phenomenon concentrated in Florida and along the coastal plain. The implication is that dynamical processes favoring mesoscale organization such as high shear associated with baroclinic circulations are more associated with higher values of extreme rain, while thermodynamic forcing and local circulations favoring isolated convection are associated with lower values of extreme rain.

Keywords: extreme precipitation; seasonal variation; precipitation organization

1. Introduction

Extreme precipitation has important societal impacts, including flooding, damage to infrastructure, and agriculture planning. The definition of the term "extreme" is somewhat arbitrary, often based on a quantile of the tail of a long-term precipitation distribution. In climatological studies, the upper 1–10% of the daily precipitation distribution has been used to define extreme rain [1–3]. In the United States, the observed increase in precipitation since the early twentieth century is mainly associated with extreme rain [1], since thunderstorms have more moisture available to produce intense precipitation as the planet warms [4]. Air temperature has been demonstrated to exert a fundamental control on the occurrence of heavy rainfall, via the Clausius-Clapeyron equation, in a modeling and observational framework [5–7]. Interannual and seasonal variability of large-scale atmospheric conditions, such as long-term climate change [8,9], the Pacific-North American (PNA) pattern [10], the El Niño-Southern Oscillation (ENSO) cycle [11], and summer monsoon dynamics [12,13], influence seasonal to decadal changes in extreme rain. Regional to local spatial patterns of extreme rainfall are tied to orographic enhancement [14], coastal geography [15], atmospheric rivers [16], and soil moisture feedbacks [17].

Studies of the linkage between extreme rainfall and the mesoscale organization of precipitation generally focus on the largest systems such as tropical cyclones [9] and mesoscale convective complexes [18]. There have been few climatological investigations of the occurrence of extreme

rainfall across the spectrum of mesoscale organization including isolated convective storms [19], despite the assessment that a main limitation in simulations of future trends in extreme precipitation is that the models do not adequately resolve convective and mesoscale precipitation processes in clouds [20–22]. A study of the simulated mechanisms of extreme precipitation in a warmer world [23] suggested that changes in vertical velocity may dominate over water vapor content in increasing precipitation extremes. This raises the question of the importance of precipitation organization to trends in extreme rain, since the dynamics of organized versus isolated convection are often distinct. Vertical motion in isolated convection is generally controlled by thermodynamic instability, while the interaction between environmental shear and internal circulations play a central role in generating upward motion in mesoscale precipitation systems [24].

The southeastern United States (SE U.S.) receives year-round precipitation from a variety of weather systems such as mid-latitude cyclones [25,26], tropical cyclones [27,28], sea breeze circulations [29], orographically-enhanced storms [30], and afternoon local storms [31]. Within these regimes, the spatial scale of precipitation organization is related to the environmental forcing that controls the formation of rain, as well as its diurnal and seasonal variation. For example, mesoscale convective systems generally form in association with large-scale forcing from frontal circulations, short waves, or lifting ahead of an upper level trough [18,32]. Isolated thunderstorms, in contrast, often form in unstable air masses in the afternoon, enhanced by local circulations related to topography or land versus water temperature contrast, independent of large-scale dynamical forcing [33,34]. A global modeling study of the mechanisms for the upward trend in mean and extreme precipitation [2] suggested that thermodynamic forcing such as increased moisture and surface temperature dominates over dynamical forcing, for example, from increased wave activity or regional circulations.

Recently, a four-year study for the SE U.S. [35] used a size-based classification to examine the diurnal and seasonal variation of mesoscale precipitation features (MPF, larger than or equal to 100 km in spatial scale) versus isolated precipitation features (IPF, smaller than 100 km). A similar framework has been used for regional and global climatological studies of precipitation systems using surface and space-based radar observations [36–41]. A recent study of precipitation organization in the SE U.S. [35] demonstrated that this framework of precipitation organization applied to a radar precipitation dataset was able to capture important differences in the seasonal evolution in precipitation organization. By analyzing daily accumulated precipitation they found that although MPF precipitation occurred year-round, IPF precipitation showed a dramatic seasonal and diurnal cycle with a summertime maximum associated with the common occurrence of isolated summertime thunderstorms in the afternoon. In this context IPF organization, for example isolated thunderstorms, relates more to thermodynamic forcing while MPF organization, for example mesoscale convective systems or widespread frontal rain, is closely, but not always uniquely, tied to dynamical forcing [42,43].

Though isolated and mesoscale precipitation respond differently to diurnal and seasonal forcing, it is not clear whether the occurrence of extreme instantaneous rainfall would also differ in the SE U.S. Do isolated storms (IPF) produce higher extreme rain rates compared to mesoscale convection (MPF)? Does the regional pattern and frequency distribution of extreme rain for IPF and MPF change as spring transitions to summer (as the convective season begins)? The goal of the present study is to investigate these questions for the SE U.S. by applying the IPF versus MPF framework to analyze the frequency distribution of hourly pixel-based extreme rainfall for the four-year period of 2009–2012 using a radar-based precipitation dataset with high time and space resolution. The analysis concluded that compared to isolated convection, mesoscale precipitation organization is more commonly associated with higher extremes in instantaneous rainfall in the SE U.S. High extreme values tied to mesoscale organization shift eastward and toward the coasts from spring to summer, while extreme rain from isolated convection is mainly a summer phenomenon concentrated in Florida and along the coastal plain. Examining the relationship between extreme precipitation and precipitation organization is relevant to understanding mechanisms for the occurrence of extreme rain, as well as

for providing guidance and verification for modeling changes to patterns of extreme rain in current and future climate.

2. Data and Approach

Precipitation data was obtained from the high-resolution radar-based National Mosaic and Multi-sensor Quantitative Precipitation Estimation datasets (NMQ) [44], which includes instantaneous precipitation rates over the SE U.S. from 24° N–40° N, 92° W–74° W over land to nearly 200 km offshore (Figure 1). The NMQ precipitation data was constructed from the national network of next-generation Doppler Radars (NEXRAD) and terminal Doppler weather radars (TDWR) on a 0.01° × 0.01° grid, approximately 1 km horizontal pixel spacing. The radar-derived precipitation rates were adjusted with rain gage data, and subjected to rigorous quality control [44]. The NMQ data set was used in a recent four-year climatology of mesoscale and isolated precipitation organization across the southeastern U.S. [35].

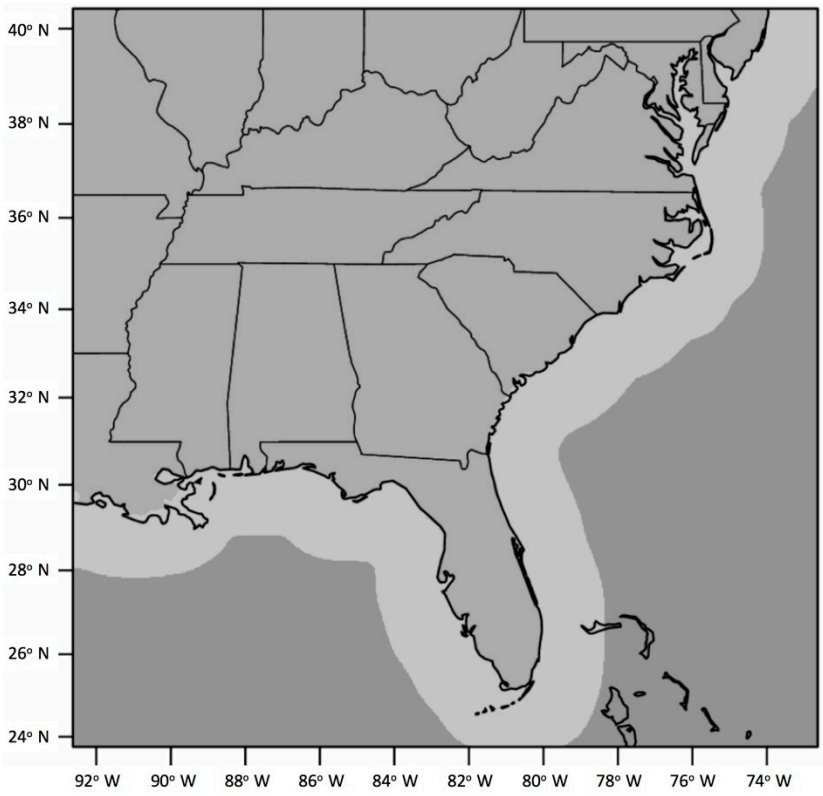

Figure 1. NMQ (National Mosaic and Multi-sensor Quantitative Precipitation Estimation datasets) radar observation domain over land (gray) and ocean (light gray). There are no radar observations in the dark gray region over the ocean.

Instantaneous rain rates were analyzed hourly from March through August for the four-year period of 2009–2012. The precipitation organization classification algorithm [35] was used to identify all rainy features in instantaneous hourly images according to feature size, as either IPF (<100 km in maximum length) or MPF (≥100 km in maximum length). A rain feature is defined as a contiguous group of pixels with instantaneous rain rate greater than or equal to 0.5 mm h^{-1} (drizzle intensity). To guide the choice of a physically-based rain rate threshold to define instantaneous extreme rain, surface radar-based climatological studies of tropical rainfall suggest radar reflectivity values of at least 40 dBZ (approximately 20 mm h^{-1}) as a first-order threshold to identify heavy rain generated from convective processes [45,46]. Rather than choose an arbitrary quantile of the rain distribution, the present study follows the well-established physical linkage between convective processes and

heavy rainfall to select an instantaneous rain rate threshold of 20 mm h^{-1} as the lower limit of extreme rain. The cumulative distribution function of all instantaneous rain values greater than or equal to 0.5 mm h^{-1} for the entire dataset (Figure 2) shows that rain rate ≥20 mm h^{-1} represent the upper 5% of all rain values. This provides a statistical justification of the choice of 20 mm h^{-1} as extreme rain for this study.

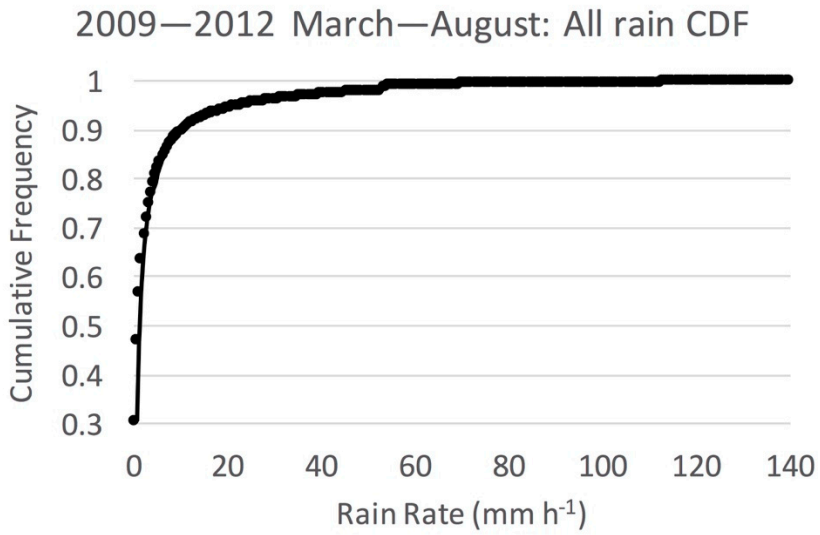

Figure 2. Cumulative frequency distribution of instantaneous rain rate ≥0.5 mm h^{-1} for the four-year data set of 2009–2012 from March–August.

The location, number, and value of extreme raining pixels were compiled once per hour for the 2009–2012 spring and summer seasons, then placed in the IPF and MPF based on the size of the associated precipitation feature as discussed earlier. From these data, the seasonal numbers of hourly extreme rain rate values for IPF and MPF were used to construct frequency distributions of extreme rain, using a bin size of 20 mm h^{-1}. These distributions were normalized by the total number of extreme rain pixels in each category, to produce relative frequency distributions independent of the number of IPF and MPF pixels. In addition, seasonal maps for the SE U.S. of the number of occurrences of instantaneous extreme rain rate each hour for IPF and MPF were produced.

3. Results

To set the stage for discussion of the distribution and spatial pattern of rain extremes, Figure 3 presents the 2009–2012 daily-averaged rain rate for the spring (March–April–May, or MAM) and summer (June–July–August, or JJA) seasons for the SE U.S. domain shown in Figure 1, separated into IPF and MPF components. The total daily-mean rain increased about 24% from spring to summer. Figure 3 shows that essentially all of the increase was in the IPF category, while MPF rain rate remained constant, demonstrating that the spring to summer precipitation transition is characterized mainly by an increase in rainfall from isolated convection. In spring, IPF accounted for 16% of the total rain, increasing to 35% in the summer, while MPF remains the dominant rain producer for both seasons.

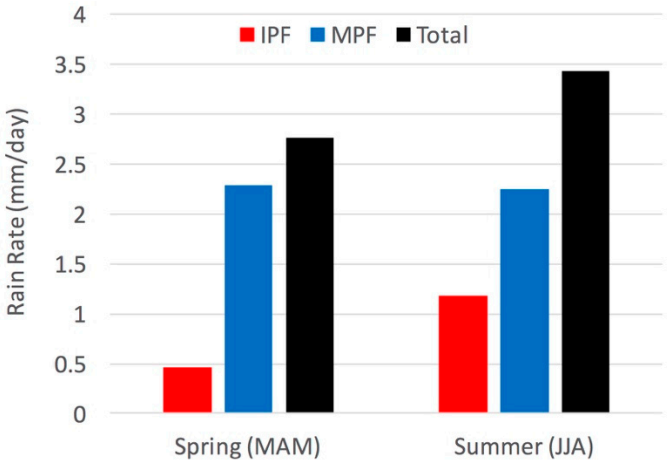

Figure 3. Mean seasonal rain rate (mm day^{-1}) during March–April–May (spring) and June–July–August (summer) over the period 2009–2012 for isolated precipitation features (IPF) (shown in red), mesoscale precipitation features (MPF) (in blue) and total (in black).

Frequency distributions, both cumulative and relative, of extreme instantaneous rain rate values for IPF and MPF over all pixels of the SE U.S. domain for 2009–2012, compiled separately for spring (MAM) and summer (JJA), are presented in Figures 4 and 5. These frequency distributions are normalized by the number of extreme raining pixels for each type, so that the distributions are independent of the absolute number of raining pixels. The cumulative distributions for spring compared to summer (Figure 4) show that in general, up to 60% of extreme rain rate values are at 20 mm h^{-1} for both seasons, while extreme values higher than 60 mm h^{-1} make up less than 10% of the total number of extreme values. In spring, MPF rain rate cumulative frequency at 20 mm h^{-1} is higher than for IPF, while between 40–80 mm h^{-1} the IPF rain rate cumulative frequency is higher than MPF. These modest differences of up to 5% in extreme rain rate cumulative frequency for IPF and MPF between 20–80 mm h^{-1} are significant to the 99% confidence level, with the significance due to the large sample size in each category (see Table 1). In summer, IPF extreme rain rates are significantly higher (to the 99% confidence level) than for MPF for all values up to 80 mm h^{-1}. These results show that on a pixel for pixel basis, the cumulative frequency of extreme instantaneous rain rate values are significantly higher for isolated convection compared to mesoscale convection in both seasons, with the exception that in the spring, mesoscale convection has higher cumulative frequency for the lowest range of extreme values. The relative frequency distributions of IPF and MPF extreme rain rate (Figure 5), which is related to the change with increasing rain rate of the cumulative distributions, display a logarithmic decrease with increasing rain rate up to 100 mm h^{-1}. Between 60–80 mm h^{-1}, the MPF relative frequency is slightly but significantly higher (to the 99% confidence level) than IPF for both seasons. Though the MPF cumulative frequency is lower in this range, the MPF relative frequency is higher.

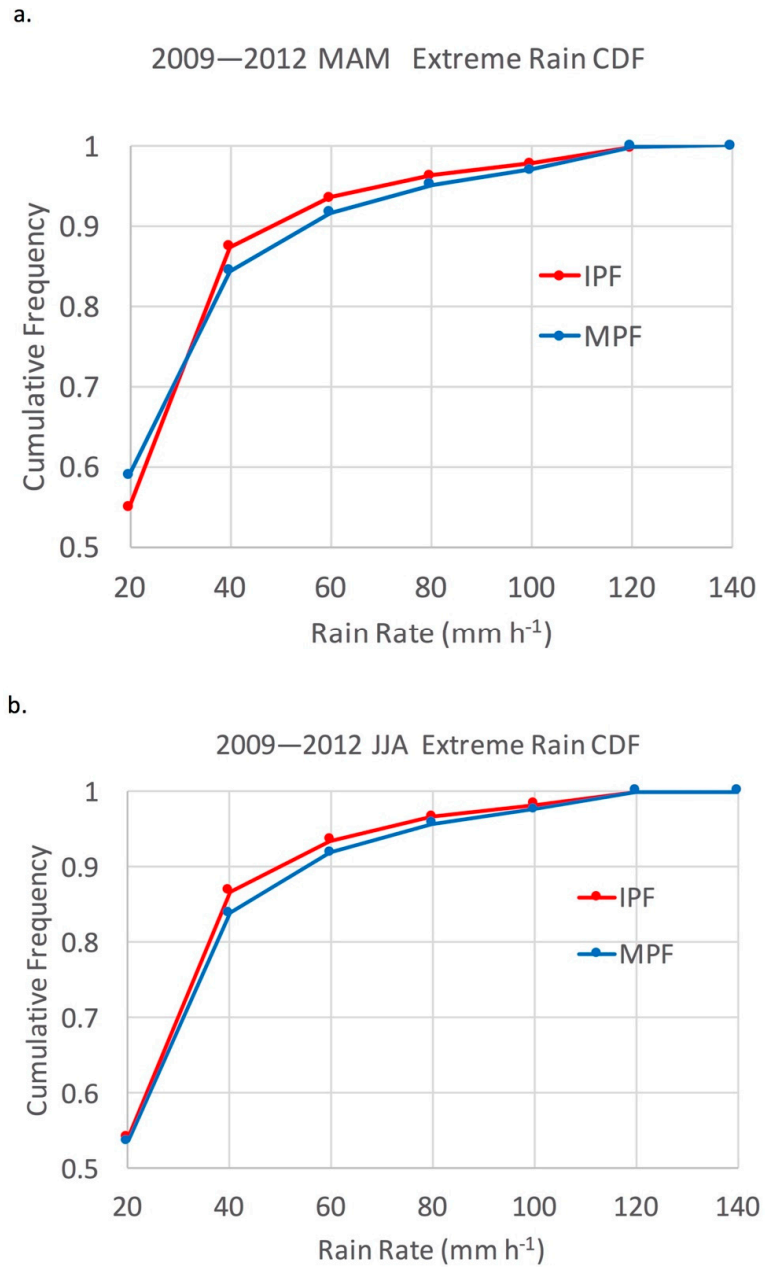

Figure 4. Cumulative frequency distribution of instantaneous extreme rain rates ($\geq$20 mm h^{-1}) sampled once per hour over all pixels for the period 2009–2012 in (**a**) March–April–May (spring) and (**b**) June–July–August (summer). IPF rain is shown in red and MPF rain in blue.

Table 1. Total number of IPF and MPF extreme rain rate pixels in the 2009–2012 sample, by season.

	SPRING (MAM)	SUMMER (JJA)
IPF	0.41×10^7	1.42×10^7
MPF	1.77×10^7	2.25×10^7

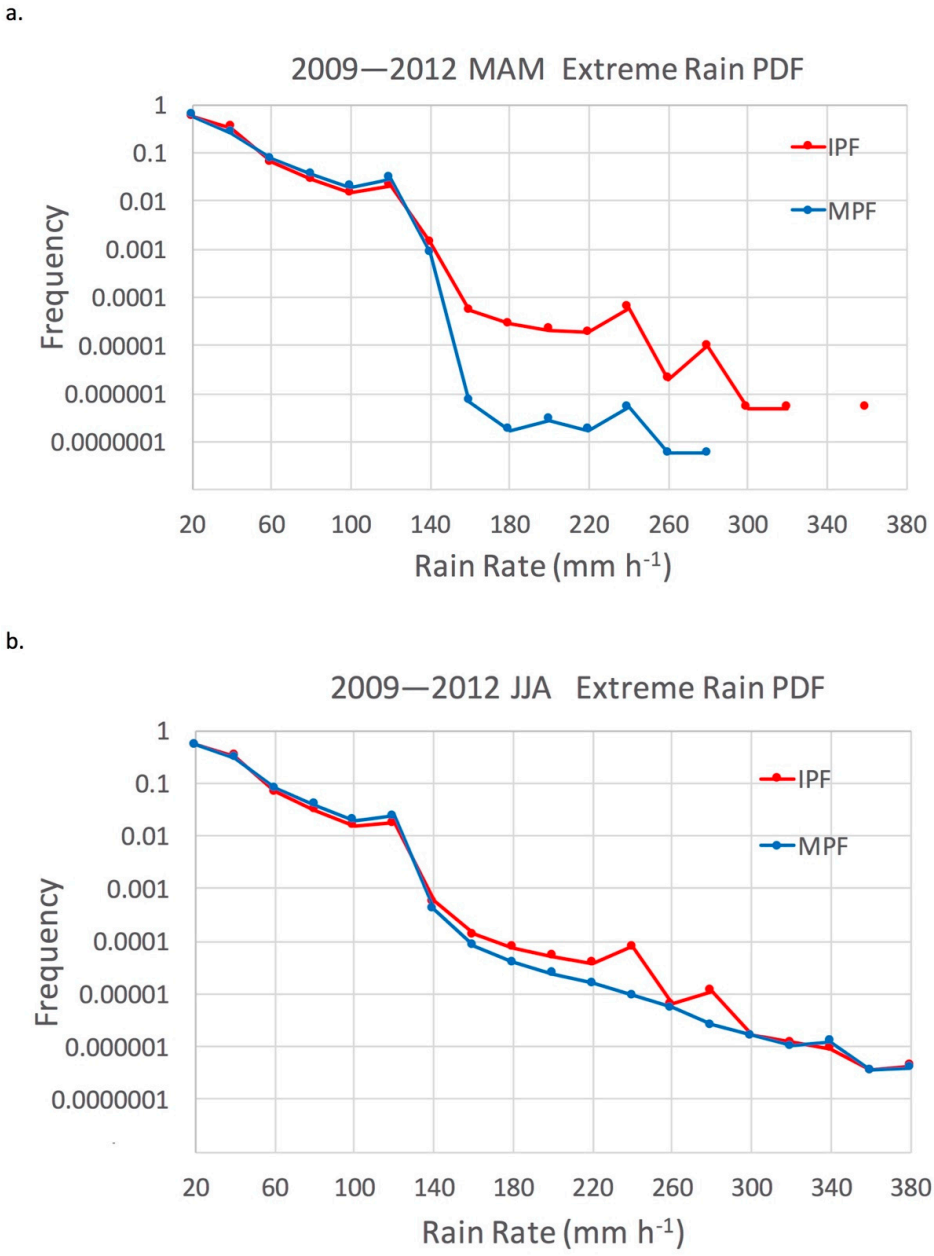

Figure 5. Relative frequency distribution of instantaneous extreme rain rates, normalized by the seasonal total of each type, for (**a**) March-April-May (spring) and (**b**) June–July–August (summer). IPF rain is shown in red and MPF rain in blue.

In other words, extreme rain is more common for isolated convection at the lower range of extreme values, while extreme rain is more common for mesoscale convection at the higher range of extreme values. This may be related to stronger vertical motion and less dry air entrainment associated with stronger dynamic forcing of the more insulated convective cores in mesoscale convection favoring higher values of extreme rainfall, compared to weaker forcing of isolated convection exposed to dry environmental air. Both IPF and MPF show a slight increase in frequency at 120 mm h^{-1} that interrupts a downward logarithmic trend. The reason for the increase at this particular rain rate value is not clear, but may be an effect of the range of each pixel to a radar which would tend to smooth and decrease the very highest rain rates at far range, and thus artificially increasing the frequency of higher rain rates near this upper limit of more common extreme rain rates. This increase is likely not due to the radar beam intersecting the bright band at far range [47], or other physically-based range effects related

to vertical reflectivity structure, since the increase is seen for both MPF and IPF (isolated convection should have no radar bright band feature). Above about 140 mm h^{-1}, the differences in IPF vs MPF relative frequency are not significant, and are exaggerated at these low frequencies by the logarithmic scale. Those differences are due to small changes to a very small number (of order 10^2 to 10^0) of extreme rain pixels in that range. Though rare, these high values are more common in the summer season. The highest measured rain rates occur between 340–380 mm h^{-1}, with about 10 pixels (out of ~10^7) showing values in that range. Instantaneous rain rate values of around 350 mm h^{-1} have been measured in hurricanes reaching land in the SE U.S. [48], so such high values of extreme rain are physically reasonable.

Maps showing the spatial pattern of the number of instantaneous extreme rain occurrences at each pixel for spring and summer over the four-year period are presented in Figures 6–8.

The pattern of total rain extreme values (Figure 6) indicates that during spring (Figure 6a), the highest frequency of extreme rain occurs in the Mississippi Valley (western edge of the domain between 90° W–88° W), and off the Carolina coast associated with the western edge of the Gulf Stream. In summer (Figure 6b), extreme rain is less frequent in the Mississippi Valley but is more common along the Gulf Coast of Florida and along the southeastern coastal plain. The maximum off the Carolina coast is particularly enhanced during the summer. The summer minus spring difference (Figure 6c) clearly shows the eastward shift with time in the occurrence of extreme rain from the inland Mississippi Valley to the southeastern coastal plain, with the largest spring to summer increase in the Florida panhandle. Note the minimum in the seasonal difference offshore along the eastern coast from Florida to North Carolina, a region with relatively little warm season rain due to suppression by the sea breeze circulation [29,35].

Similar maps of extreme rain occurrence are shown in Figures 7 and 8 but are separated into IPF and MPF components. The spatial pattern of the seasonal shift in IPF extreme rain occurrence at each pixel (Figure 7) clearly shows the summer increase across the southeastern U.S. generally, with the increase concentrated in Florida and the coastal plain, as warm, humid air from the Gulf of Mexico and Caribbean interacts with the diurnal sea breeze. In contrast, the MPF extreme rain occurrence (Figure 8) decreases in the summer across the western domain as baroclinic circulations and strong shear tend to migrate northward with the jet stream [26]. In the context of Figures 3 and 5, this suggests that although the SE U.S. average MPF rain is about the same in spring and summer, there is a larger region of higher extreme values of MPF rain in spring over the western half of the SE U.S. These results are generally consistent with the spring to summer decrease in the frequency of large, long-lived nocturnal mesoscale convective systems west of the Appalachian Mountains, as well as with the climatology of atmospheric river interactions with the SE U.S. coast [30,49–51].

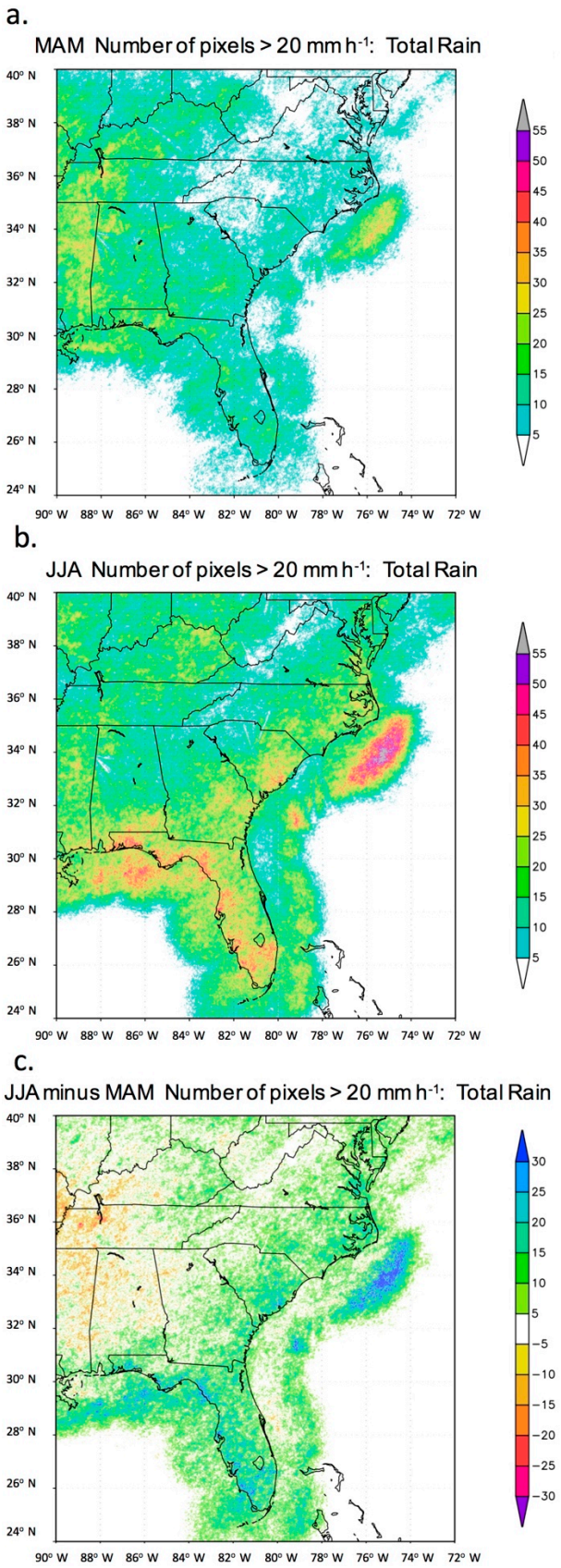

Figure 6. The number of occurrences at each pixel of instantaneous total rain rate >20 mm h^{-1} sampled once every hour over 2009–2012 for (**a**) March–April–May (MAM, spring), (**b**) June–July–August (JJA, summer), and (**c**), the summer minus spring difference (JJA–MAM).

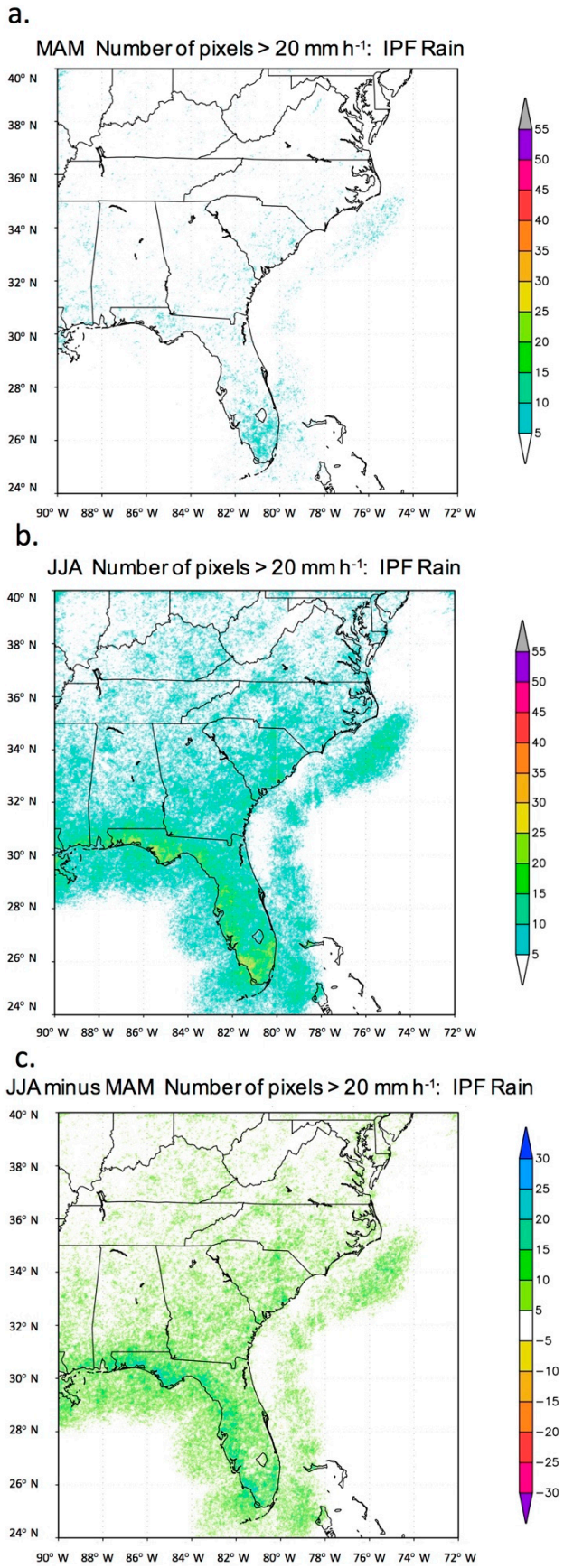

Figure 7. The number of occurrences at each pixel of instantaneous IPF rain rate >20 mm h^{-1} sampled once every hour over 2009–2012 for (**a**) March–April–May (MAM, spring), (**b**) June–July–August (JJA, summer), and (**c**), the summer minus spring difference (JJA–MAM).

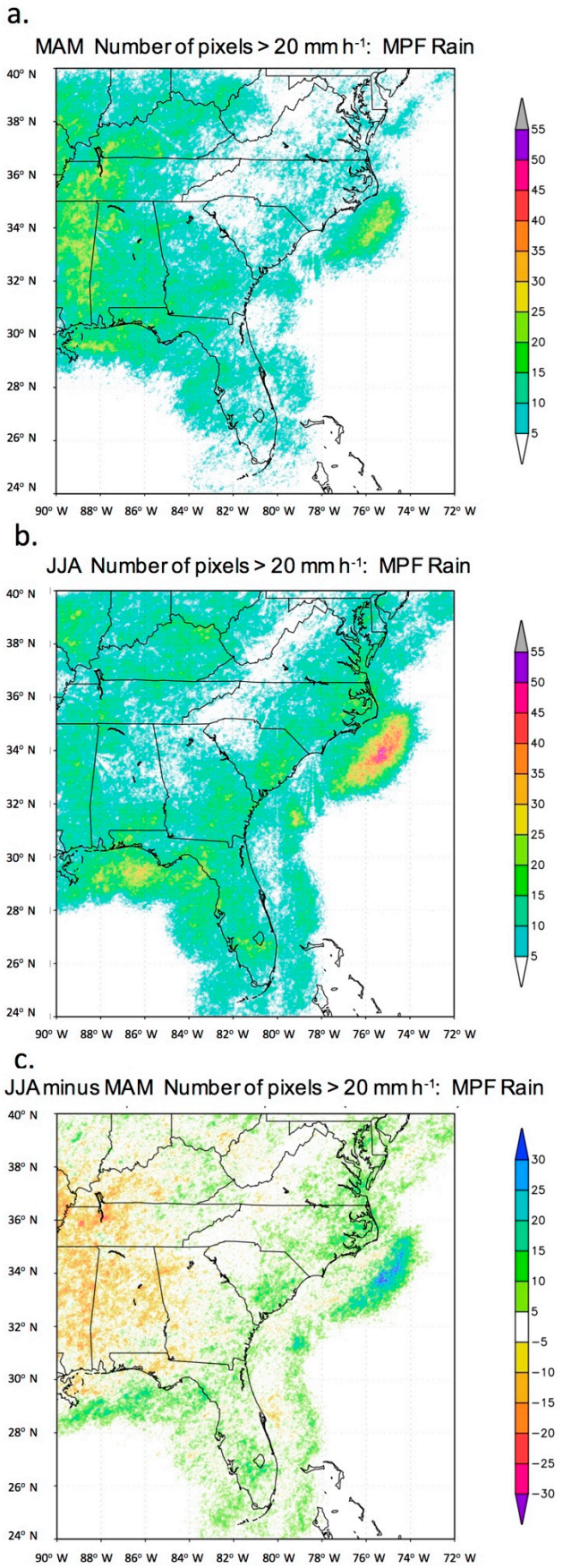

Figure 8. The number of occurrences at each pixel of instantaneous MPF rain rate >20 mm h^{-1} sampled once every hour over 2009–2012 for (**a**) March–April–May (MAM, spring), (**b**) June–July–August (JJA, summer), and (**c**), the summer minus spring difference (JJA–MAM).

4. Summary and Conclusions

This study focuses on the association between instantaneous extreme precipitation and mesoscale organization of the precipitation during the spring to summer transition over the southeastern United States in a four-year surface radar precipitation data set. This research examines whether isolated precipitation features (IPF) have a distinct distribution and spatial pattern of extreme rain compared to mesoscale precipitation features (MPF), and how these distributions and spatial patterns change from spring to summer. Since isolated and mesoscale precipitation have different synoptic and seasonal forcing mechanisms, the results of this work may help advance the question of whether thermodynamic or dynamic processes dominate the occurrence of extreme rain in the southeastern United States.

Extreme precipitation is defined in this study as instantaneous values of rain rate of at least 20 mm h^{-1}, which generally corresponds to heavy rainfall generated by convective processes. Rain rate at each pixel of the NMQ surface radar-based dataset over the SE U.S. was sampled once per hour and compiled for spring and summer in the period 2009–2012. Contiguous precipitation features were objectively identified each hour and placed in either the IPF (<100 km in maximum length) or MPF ($\geq$100 km in maximum length). Statistically significant differences between the IPF and MPF cumulative and relative frequency distributions suggested that the cumulative frequency of extreme instantaneous rain rate values are higher for IPF compared to MPF in both seasons, with the exception that in the spring, mesoscale convection has greater cumulative frequency for the lowest range of extreme values likely associated with large springtime mesoscale convective systems. The relative frequency distributions further reveal that at the lower range of extreme rain (which dominates the cumulative frequency since lower values are more common), the relative frequency of IPF is greater than MPF, while at the higher range of extreme values the relative frequency of MPF extrema are greater than for IPF. The highest values of extreme rain, in the 340–380 mm h^{-1} range, are extremely rare (of the order 10 out of 10^7 samples) and occur for both IPF and MPF.

The spatial pattern over the SE U.S. of the number of extreme values at each pixel shows that although the SE U.S. average MPF rainfall is about the same in spring and summer, there is a larger region of higher extreme values of MPF rain over the Mississippi Valley in the western half of the SE U.S. domain, where previous studies show that large mesoscale convective systems tend to occur. The IPF extreme rain occurrence has a dramatic increase from spring to summer, mainly in Florida and along the coastal plain. The highest concentration of extreme rain occurs for summer MPF offshore of the Carolinas on the western edge of the warm Gulf Stream current, where previous studies suggest that a continuous supply of moisture from the warm ocean surface is lifted by nocturnal ascent in the diurnal sea breeze circulation [29,34]. Although extreme MPF rain is concentrated offshore, there is some ambiguity as to whether the statistical difference in the extreme rain distribution is due to land versus ocean differences, which is an important distinction from a risk analysis perspective. A more detailed analysis of land versus ocean extremes is left for future work.

In summary, these results show that although isolated convection is more commonly associated with lower extreme rain rates (20–60 mm h^{-1}), the higher extreme rain rates between 60–80 mm h^{-1} in the SE U.S. are more commonly tied to mesoscale organization. The frequency differences for IPF and MPF extrema are significant to the 99% confidence level. The implication is that dynamical processes favoring mesoscale organization such as high shear associated with baroclinic circulations are more likely to produce higher values of extreme rain, while thermodynamic forcing and local circulations favoring isolated convection are more commonly associated with lower values of extreme rain. High extreme values tied to mesoscale organization shift eastward and toward the coasts from spring to summer, while extreme rain from isolated convection is mainly a summer phenomenon concentrated in Florida and along the coastal plain. One hypothesis to explain these results is that stronger vertical motion and less dry air entrainment are associated with stronger dynamic forcing of the more insulated convective cores of mesoscale convection, leading to a higher frequency of extreme rain values. An insulating region of moist air surrounding clusters of convective cells has been found to reduce the detrimental effects of dry air entrainment on parcel buoyancy [52]. Weaker forcing

of isolated convection exposed to drier environmental air may limit the extreme rain rates for IPF. In future work, these mechanisms may be tested in high resolution mesoscale model simulations of spring and summer precipitation.

Funding: This research was funded by a grant (AGS-1660049) from the National Science Foundation (United States) Climate and Large-Scale Dynamics program and the Physical and Dynamic Meteorology program in the Division of Atmospheric and Geospatial Science.

Acknowledgments: The anonymous reviewers are acknowledged for their insightful comments that greatly improved the manuscript.

Conflicts of Interest: The author declares no conflict of interest. The funding sponsors had no role in the design of the study; in the collection, analyses, or interpretation of data; in the writing of the manuscript, and in the decision to publish the results.

References

1. Karl, T.; Knight, R.W. Secular trends of precipitation amount, frequency, and intensity in the United States. *Bull. Am. Meteorol. Soc.* **1998**, *79*, 231–242. [CrossRef]
2. Emori, S.; Brown, S.J. Dynamic and thermodynamic changes in mean and extreme precipitation under changed climate. *Geophys. Res. Lett.* **2005**, *32*. [CrossRef]
3. Wang, Y.; Zhou, L. Observed trends in extreme precipitation events in China during 1961–2001 and the associated changes in large-scale circulation. *Geophys. Res. Lett.* **2005**, *32*. [CrossRef]
4. Trenberth, K. Changes in precipitation with climate change. *Clim. Res.* **2011**, *47*, 123–138. [CrossRef]
5. Allen, M.; Ingram, W. Constraints on future changes in climate and the hydrologic cycle. *Nature* **2002**, *419*, 224–232. [CrossRef] [PubMed]
6. Allan, R.; Soden, B. Atmospheric warming and the amplification of precipitation extremes. *Science* **2008**, *321*, 1481–1484. [CrossRef] [PubMed]
7. Liu, S.C.; Fu, C.; Shiu, C.J.; Chen, J.P.; Wu, F. Temperature dependence of global precipitation extremes. *Geophys. Res. Lett.* **2009**, *36*, L17702. [CrossRef]
8. Trenberth, K. Conceptual framework for changes of extremes of the hydrological cycle with climate change. *Clim. Chang.* **1999**, *42*, 327–339. [CrossRef]
9. Kunkel, K.; Easterling, D.; Kristovich, D.; Gleason, B.; Stoecker, L.; Smith, R. Recent increases in U.S. heavy precipitation associated with tropical cyclones. *Geophys. Res. Lett.* **2010**, *37*, L24706. [CrossRef]
10. Mock, C. Climatic controls and spatial variations of precipitation in the western United States. *J. Clim.* **1996**, *9*, 1111–1125. [CrossRef]
11. Curtis, S.; Salahuddin, A.; Adler, R.; Huffman, G.; Gu, G.; Hong, Y. Precipitation extremes estimated by GPCP and TRMM: ENSO relationships. *J. Hydrometeorol.* **2007**, *8*, 678–689. [CrossRef]
12. Gadgil, S.; Vinayachandran, P.; Francis, P.; Gadgil, S. Extremes of the Indian summer monsoon rainfall, ENSO and equatorial Indian Ocean oscillation. *Geophys. Res. Lett.* **2004**, *31*. [CrossRef]
13. Boers, N.; Bookhagen, B.; Marwan, N.; Kurths, J.; Marengo, J. Complex networks identify spatial patterns of extreme rainfall events of the South American Monsoon System. *Geophys. Res. Lett.* **2013**, *40*, 4386–4392. [CrossRef]
14. Xu, W.; Zipser, E.; Chen, Y.L.; Liu, C.; Liou, Y.C.; Lee, W.C.; Jou, B.J. An orography-associated extreme rainfall event during TiMREX: Initiation, storm evolution, and maintenance. *Mon. Weather Rev.* **2012**, *140*, 2555–2574. [CrossRef]
15. Mapes, B.; Warner, T.; Xu, M.; Negri, A. Diurnal patterns of rainfall in northwestern South America. Part I: Observations and context. *Mon. Weather Rev.* **2003**, *131*, 799–812. [CrossRef]
16. Ralph, F.M.; Dettinger, M. Historical and national perspectives on extreme west coast precipitation associated with atmospheric rivers during December 2010. *Bull. Am. Meteorol. Soc.* **2012**, *93*, 783–790. [CrossRef]
17. Hohenegger, C.; Brockhaus, P.; Bretherton, C.; Schär, C. The soil moisture-precipitation feedback in simulations with explicit and parameterized convection. *J. Clim.* **2009**, *22*, 5003–5020. [CrossRef]
18. Laing, A.; Fritsch, J.; Negri, A. Contribution of mesoscale convective complexes to rainfall in Sahelian Africa: Estimates from geostationary infrared and passive microwave data. *J. Appl. Meteorol. Climatol.* **1999**, *38*, 957–964. [CrossRef]

19. Nesbitt, S.W.; Zipser, E.J. The diurnal cycle of rainfall and convective intensity according to three years of TRMM measurements. *J. Clim.* **2003**, *16*, 1456–1475. [CrossRef]
20. Schiermeier, Q. The real holes in climate science. *Nature* **2010**, *463*, 284–287. [CrossRef] [PubMed]
21. Kao, S.-C.; Ganguly, A. Intensity, duration and frequency of precipitation extremes under 21st century warming scenarios. *J. Geophys. Res.* **2011**, *116*, D16119. [CrossRef]
22. Hourdin, F.; Grandpeix, J.-Y.; Rio, C.; Bony, S.; Jam, A.; Cheruy, F.; Rochetin, N.; Fairhead, L.; Idelkadi, A.; Musat, I.; et al. LMDZ5B: The atmospheric component of the IPSL climate model with revisited parameterizations for clouds and convection. *Clim. Dyn.* **2013**, *40*, 2193–2222. [CrossRef]
23. O'Gorman, P.; Schneider, T. The physical basis for increases in precipitation extremes in simulations of 21st century climate change. *Proc. Natl. Acad. Sci. USA* **2009**, *106*, 14773–14777. [CrossRef] [PubMed]
24. Houze, R. Observed structure of mesoscale convective systems and implications for large-scale heating. *Q. J. R. Meteorol. Soc.* **1989**, *115*, 425–461. [CrossRef]
25. Curtis, S. Developing a climatology of the South's 'other' storm season: ENSO impacts on winter extratropical cyclogenesis. *Southeast. Geogr.* **2006**, *46*, 231–244. [CrossRef]
26. Nieto Ferreira, R.; Hall, L.; Rickenbach, T. A climatology of the structure, evolution and propagation of midlatitude cyclones in the southeast United States. *J. Clim.* **2013**, *26*, 8406–8421. [CrossRef]
27. Larson, J.; Zhou, Y.; Higgins, R.W. Characteristics of landfalling tropical cyclones in the United States and Mexico: Climatology and interannual variability. *J. Clim.* **2005**, *18*, 1247–1262. [CrossRef]
28. Shepherd, J.M.; Grundstein, A.; Mote, T. Quantifying the contribution of tropical cyclones to extreme rainfall along the coastal southeastern United States. *Geophys. Res. Lett.* **2007**, *34*, L23810. [CrossRef]
29. Koch, S.; Ray, C. Mesoanalysis of summertime convergence zones in central and eastern North Carolina. *Weather Forecast.* **1997**, *12*, 56–77. [CrossRef]
30. Parker, M.D.; Ahijevych, D.A. Convective episodes in the east-central United States. *Mon. Weather Rev.* **2007**, *135*, 3707–3727. [CrossRef]
31. Winkler, J.A.; Skeeter, B.R.; Yamamoto, P.D. Seasonal variations in the diurnal characteristics of heavy hourly precipitation across the United States. *Mon. Weather Rev.* **1988**, *116*, 1641–1658. [CrossRef]
32. Leary, C.; Houze, R. The structure and evolution of convection in a tropical cloud cluster. *J. Atmos. Sci.* **1979**, *36*, 437–457. [CrossRef]
33. Wallace, J. Diurnal variations in precipitation and thunderstorm frequency over the conterminous United States. *Mon. Weather Rev.* **1975**, *103*, 406–419. [CrossRef]
34. Carbone, R.; Tuttle, J. Rainfall occurrence in the U.S. warm season: The diurnal cycle. *J. Clim.* **2008**, *21*, 4132–4146. [CrossRef]
35. Rickenbach, T.M.; Nieto-Ferreira, R.; Zarzar, C.; Nelson, B. A seasonal and diurnal climatology of precipitation organization in the southeastern United States. *Q. J. R. Meteorol. Soc.* **2015**, *141*, 1938–1956. [CrossRef]
36. Rickenbach, T.M.; Rutledge, S.A. Convection in TOGA COARE: Horizontal scale, morphology and rainfall production. *J. Atmos. Sci.* **1998**, *55*, 2715–2729. [CrossRef]
37. Nesbitt, S.W.; Zipser, E.J.; Cecil, D.J. A census of precipitation features in the tropics using TRMM: Radar, ice scattering, and lightning observations. *J. Clim.* **2000**, *13*, 4087–4106. [CrossRef]
38. Nesbitt, S.W.; Cifelli, R.; Rutledge, S.A. Storm morphology and rainfall characteristics of TRMM precipitation features. *Mon. Weather Rev.* **2006**, *134*, 2702–2721. [CrossRef]
39. Rickenbach, T.M.; Nieto-Ferreira, R.; Barnhill, R.; Nesbitt, S. Regional contrast of mesoscale convective system structure prior to and during monsoon onset across South America. *J. Clim.* **2011**, *24*, 3753–3763. [CrossRef]
40. Rickenbach, T.M.; Nieto-Ferreira, R.; Barnhill, R.; Nesbitt, S. Seasonal and regional differences in the rainfall and intensity of isolated convection over South America. *Int. J. Climatol.* **2013**, *33*, 2002–2007. [CrossRef]
41. Liu, C.; Zipser, E. Regional variation of morphology of organized convection in the tropics and subtropics. *J. Geophys. Res. Atmos.* **2013**, *118*, 453–466. [CrossRef]
42. Keenan, T.D.; Carbone, R.E. A preliminary morphology of precipitation systems in tropical northern Australia. *Q. J. R. Meteorol. Soc.* **1992**, *118*, 283–326. [CrossRef]
43. Miller, P.; Mote, T. A climatology of weakly forced and pulse thunderstorms in the Southeast United States. *J. Appl. Meteorol. Climatol.* **2017**, *56*, 3017–3033. [CrossRef]

44. Zhang, J.; Howard, K.; Vasiloff, S.; Langston, C.; Kaney, B.; Arthur, A.; Van Cooten, S.; Kelleher, K.; Kitzmiller, D.F.; Ding, F. National Mosaic and QPE (NMQ) System: description, results, and future plans. *Bull. Am. Meteorol. Soc.* **2011**, *92*, 1321–1338. [CrossRef]
45. Steiner, M.; Houze, R.; Yuter, S. Climatological characterization of three-dimensional storm structure from operational radar and rain gauge data. *J. Appl. Meteorol.* **1995**, *34*, 1978–2007. [CrossRef]
46. Marks, D.; Wolff, D.; Silberstein, D.; Tokay, A.; Pippitt, J.; Wang, J. Availability of high-quality TRMM ground validation data from Kwajalein, RMI: A practical application of the relative calibration adjustment technique. *J. Atmos. Ocean. Technol.* **2009**, *26*, 413–429. [CrossRef]
47. Fabry, F.; Austin, G.; Tees, D. The accuracy of rainfall estimates by radar as a function of range. *Q. J. R. Meteorol. Soc.* **1992**, *118*, 435–453. [CrossRef]
48. Medlin, J.; Kimball, S.; Blackwell, K. Radar and rain gauge analysis of the extreme rainfall during Hurricane Danny's (1997) landfall. *Mon. Weather Rev,* **2007**, *135*. [CrossRef]
49. Maddox, R. Mesoscale convective complexes. *Bull. Am. Meteorol. Soc.* **1980**, *61*, 1374–1387. [CrossRef]
50. Laing, A.; Fritsch, J. The global population of mesoscale convective complexes. *Q. J. R. Meteorol. Soc.* **1997**, *123*, 389–405. [CrossRef]
51. Debbage, N.; Miller, P.; Poore, S.; Morano, T.; Mote, T.; Shepherd, J.M. A climatology of atmospheric river interactions with the southeastern United States coastline. *Int. J. Climatol.* **2017**, *37*, 4077–4091. [CrossRef]
52. Becker, T.; Bretherton, C.; Hohenegger, C.; Stevens, B. Estimating bulk entrainment with unaggregated and aggregated convection. *Geophys. Res. Lett.* **2018**, *45*, 455–462. [CrossRef]